ANL-6280

ANL-6280

Argonne National Laboratory

AN ULTRASONIC MEASUREMENT SYSTEM FOR THE PRECISE DETERMINATION OF THE ELASTIC MODULI OF SINGLE CRYSTALS

by

C. J. Renken

DISCLAIMER

Price 50 Cents . *Available from the Office of Technical Services, Department of Commerce, Washington 25, D.C.*

ANL-6280
Engineering and Equipment
(TID-4500, 16th Ed.)
AEC Research and
Development Report

ARGONNE NATIONAL LABORATORY
9700 South Cass Avenue
Argonne, Illinois

AN ULTRASONIC MEASUREMENT SYSTEM FOR THE PRECISE DETERMINATION OF THE ELASTIC MODULI OF SINGLE CRYSTALS

by

C. J. Renken

Metallurgy Division

Program 12.1.1

Portions of the material in this report have appeared in the following Metallurgy Division Annual report

ANL-6099 - page 55 - December 1959

May 1961

Operated by The University of Chicago
under
Contract W-31-109-eng-38

TABLE OF CONTENTS

LIST OF FIGURES

AN ULTRASONIC MEASUREMENT SYSTEM FOR THE PRECISE DETERMINATION OF THE ELASTIC MODULI OF SINGLE CRYSTALS

by

C. J. Renken

The measurement of the ultrasonic wave velocities in a sufficient number of known directions in a single crystal makes possible the direct computation of the elastic moduli of the crystal. For specimens having linear dimensions on the order of 2 to 3 mm, phase comparison techniques have been found useful. The equipment described in this paper is based on the technique developed by McSkimin.(1) The measurement system is actually a type of acoustic interferometer adapted to small solid specimens, and it requires specialized electronic equipment which cannot be purchased off the shelf. Therefore it was decided to design and construct this system to include the features of convenience and flexibility necessary in a permanent piece of equipment.

I. Features of the System

Figure 1 shows a block diagram of the system. Briefly, radiofrequency (rf) pulses of a known frequency are generated and converted into pressure variations by a quartz crystal. These pressure waves propagate down a fused quartz or crystal quartz buffer rod toward the specimen. The couplant between the buffer and specimen transmits part of the energy into the specimen; most of the remaining energy is reflected back from the buffer-couplant-specimen interface. The oscilloscope presentation with no specimen present appears as shown in Figure 2a. The energy traveling in the specimen is reflected back and forth between the specimen faces. During each round trip, part of the energy is transmitted back through the couplant into the buffer rod. At discrete frequencies, the pattern appears as shown in Figure 2b. When this occurs, the specimen waves are all in phase, but out of phase with the interface reflection. The velocity of propagation is given by

$$v = \frac{2tf}{n + (\gamma/360)}$$

where

f = frequency
t = specimen thickness
n = number of waves
γ = couplant correction.

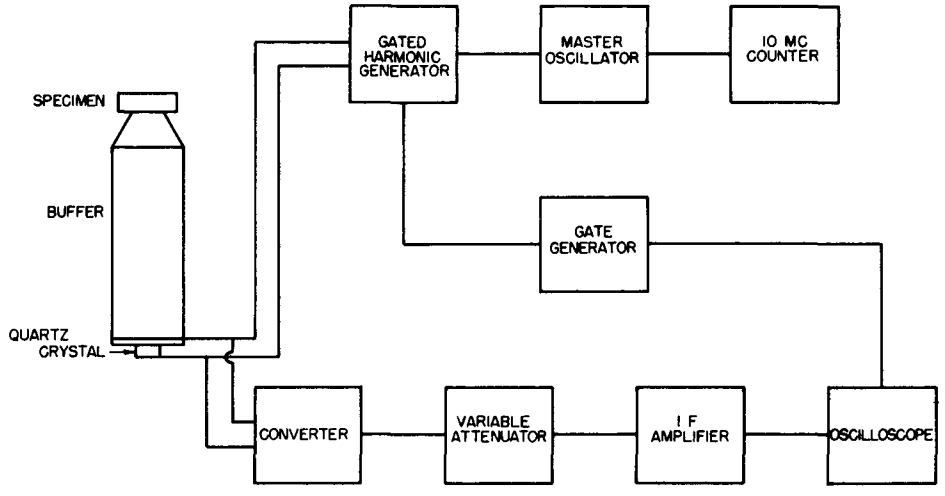

Figure 1

Block Diagram of the System

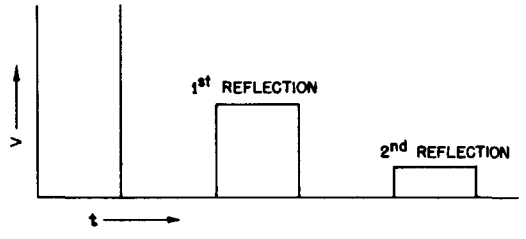

Figure 2a

An Idealized Oscilloscope Presentation When No Specimen Is Coupled to the Active Area of the Buffer

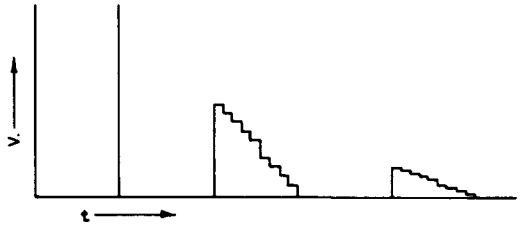

Figure 2b

An Idealized Oscilloscope Presentation When the Specimen Waves Are All in Phase, But out of Phase with the Interface Reflection

The couplant correction may be determined from a knowledge of the magnitude of the interface reflection and first reflection from the far end of the specimen as they appear at the quartz crystal end of the buffer. This was shown in an analysis mentioned in Appendix B of Ref. 1. The correctness of this analysis has been corroborated,and details are given in the Appendix of this report.

II. Circuit Design Features

A. Gate Generator Section

The circuit diagram of the gate generator section is shown in Figure 3. A rate generator triggers a thyratron which produces the trigger pulses for the oscilloscope and the gate generator. The gate generator

produces a square pulse with a rise time of 0.1 μsec and a decay time of 0.3 μsec. The duration of this pulse can be varied from 1 to 50 μsec. The gate pulse is power amplified and appears at the output of this section as a square pulse of 400-volt amplitude and with a peak power of 5 watts.

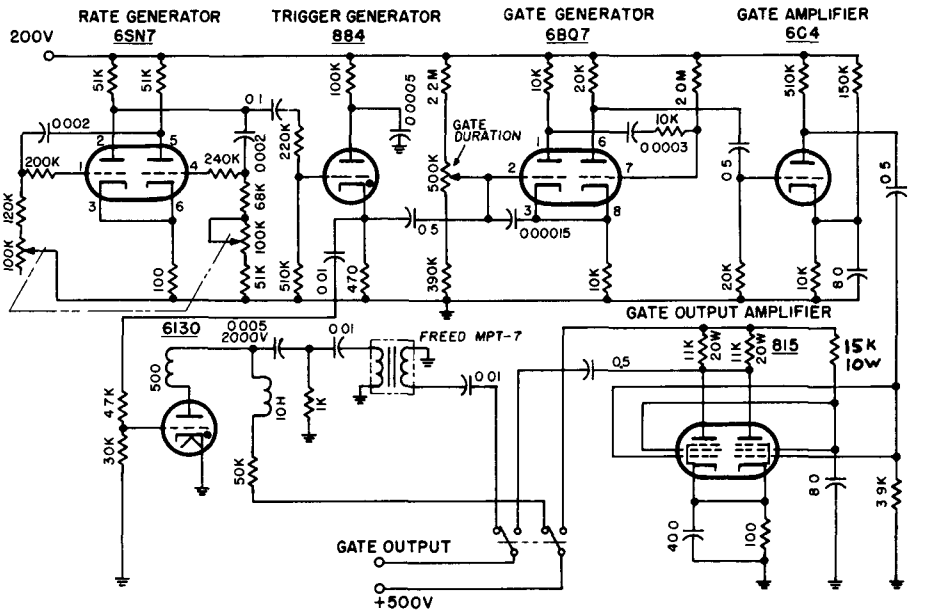

Figure 3

The Circuit Diagram of the Gage Generator Section

B. Master Oscillator

The master oscillator section, shown in Figure 4, generates the fundamental frequency which controls all the later stages. High stability and low harmonic output are the fundamental requirements. A high-C Hartley circuit is used because of the wide frequency range which must be covered. This is followed by two buffer stages which filter out harmonics and generate the power necessary to operate efficiently the succeeding harmonic generators. The tuned circuits of the oscillator and buffer are all ganged with and track with the harmonic generators so that one shaft tunes everything simultaneously.

C. The Gated Harmonic Generator

The gated harmonic generator section shown in Figure 5 produces the pulses of rf energy which drive the quartz crystal transducer. Output is available over a continuous frequency range from 16 to 144 megacycles per second. This wide frequency range is useful to minimize and evaluate dispersion due to the effects of diffraction in the small specimens customarily available.

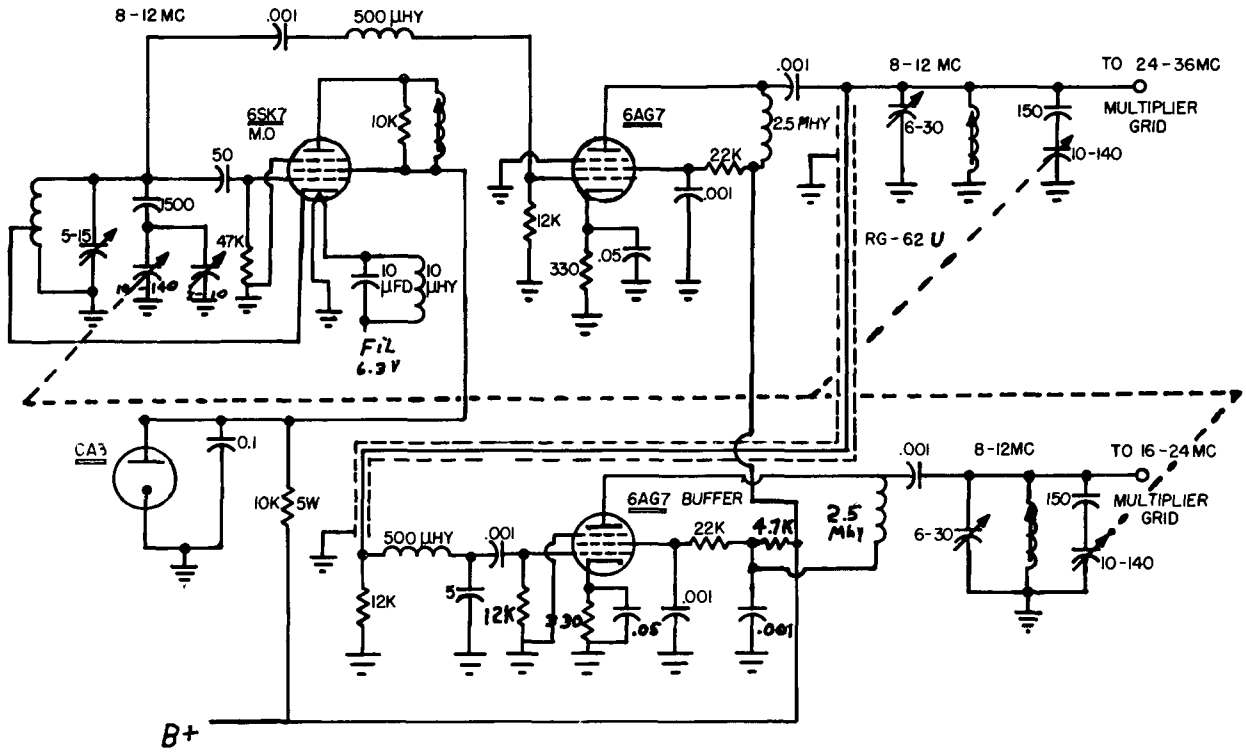

Figure 4

The Circuit Diagram of the Master Oscillator Section

The gated harmonic generator is divided into two banks. The first stage doubles in the first stage and every stage thereafter to give 16-24, 32-48 and 64-96 Mc; the second bank triples in the first stage and doubles from then on to give 24-36, 48-72 and 96-144 Mc. The harmonic generators are beam tetrodes type 5763, gated in the screen circuit. The gate pulse alternates from one bank to the other as the various ranges are traversed.

When a stage is delivering output to the crystal, the cathode of the succeeding stage is held above ground to avoid loading down the working stage. These functions are accomplished in the band switch. About 5 watts peak are available to drive the quartz transducer on the top range (96-144 Mc). The gating of the harmonic generators must be exceptionally effective. This means that a special effort must be made to keep oscillator harmonics out of the tank circuit of the harmonic generator section in use. This leakage must be 80 db down from the rf peak pulse amplitude in all stages.

D. The Converter Section

The converter section is shown in Figures 6 and 7. The reflections coming from the active area of the buffer rod are relatively weak and must be amplified to be useful.

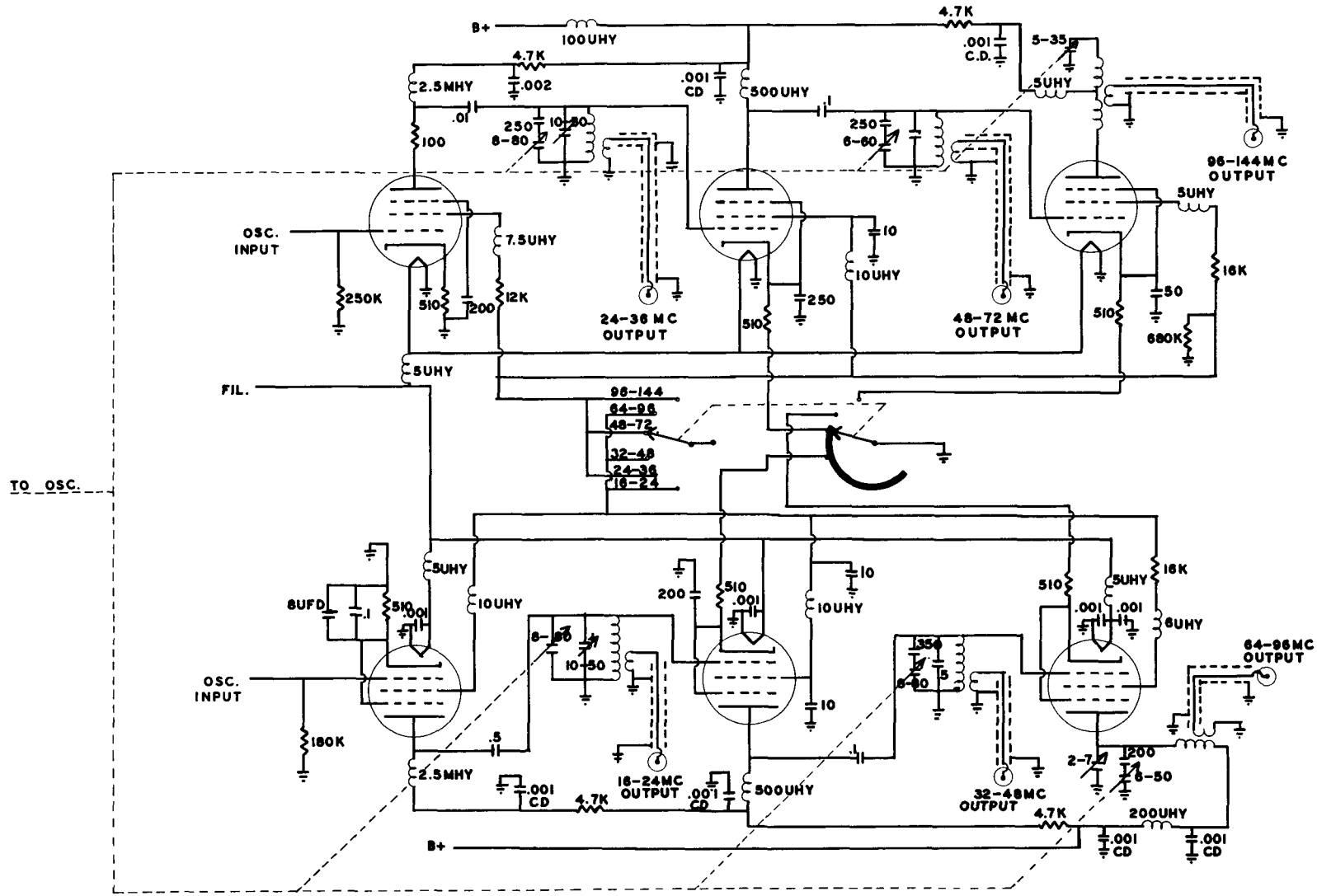

Figure 5

The Circuit Diagram of the Gated Harmonic Generator

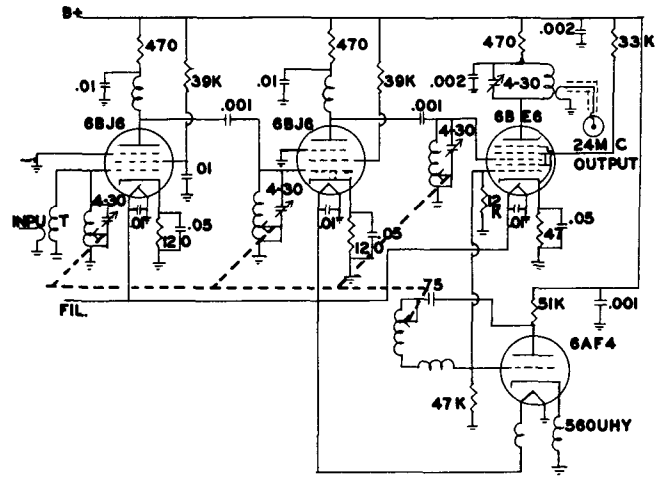

Figure 6

The Circuit Diagram of the Converter Section, 40-150 Mc

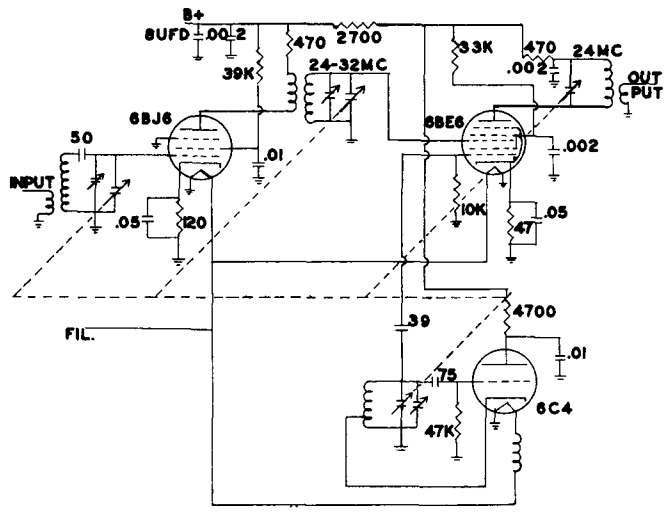

Figure 7

The Type of Circuit Used for the 20, 30, and 36-Mc Converters

This is accomplished by a set of tunable converters operating over various frequency ranges, and a fixed frequency I.F. amplifier. The range from 40 to 150 Mc is covered by a converter tuned by a spiral inductuner; the range below this frequency is covered by several conventional converters using fixed L, variable C-tuned circuits.

Between the converter and I.F. amplifier is inserted a variable attenuator. Accurate calibration is not necessary for the measurement of velocities. The design is simplified by the fact that the attenuator operates at a fixed frequency.

E. The I.F. Amplifier

The I.F. amplifier and attenuator are shown in Figures 8a and 8b. The I.F. amplifier must amplify the signals from the converter to a level sufficient for rectification. This string of amplifiers is designed to have sufficient bandwidth to preserve the proper pulse shape and to recover rapidly when overdriven.

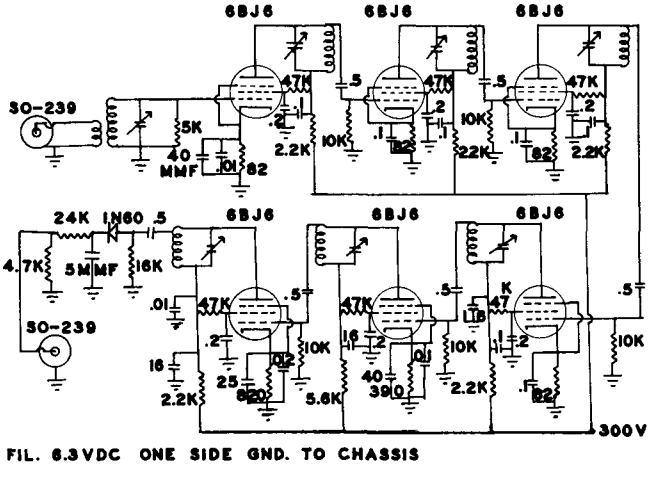

Figure 8a

The Circuit Diagram of the I. F. Amplifier

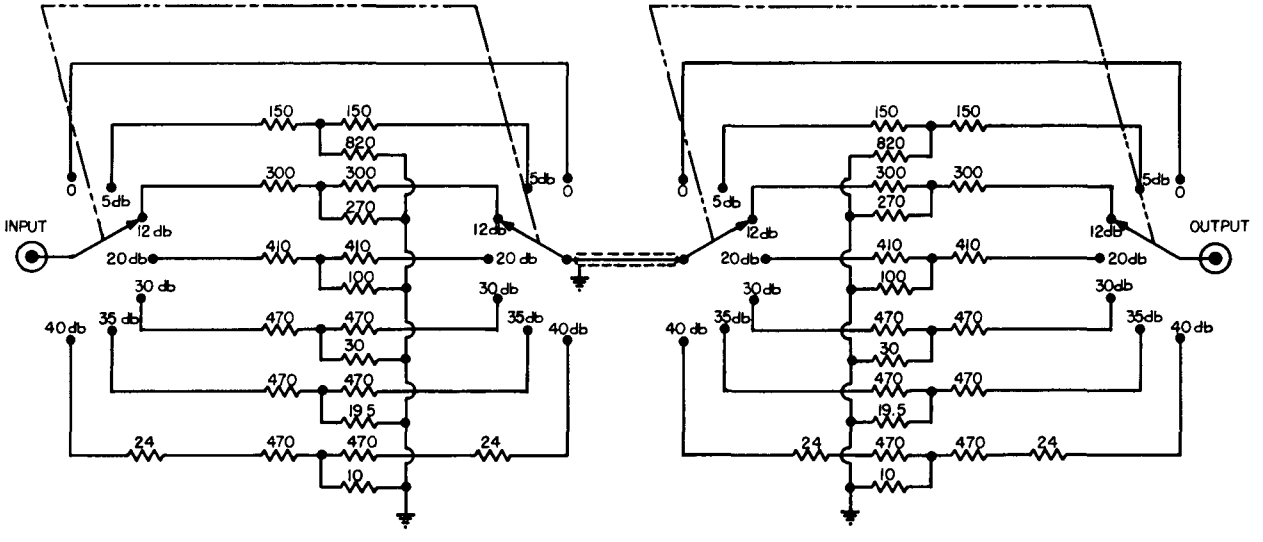

Figure 8b

The Circuit Diagram of the I.F. Attenuator

The initial rf pulse impressed across the quartz crystal may have an amplitude 40 db or more above the first echo. The I.F. section must recover completely from this overload before the arrival of the echo from the active area of the buffer. The I.F. amplifier shown in the circuit diagram has a bandwidth of 4 Mc centered around 23 Mc.

F. Buffer Rods

The buffer rods used in this measurement system are essentially ultrasonic delay lines, which are thoroughly discussed in many publications.(2) The area of the buffer rod parallel to the quartz crystal is usually a small square, approximately 2 mm on a side. It is formed by beveling the end of the buffer at a 30° angle to the plane of the active area. The only ultrasonic energy reaching the specimen passes through the active area, which must be at least as small as the specimen in order for the analysis for the phase shift in the couplant to be valid. It might be mentioned that ordinary domestic fused quartz is satisfactory for frequencies below 60 Mc, but becomes increasingly lossy above that frequency. Above 60 Mc, #1 optical grade fused quartz or equivalent should be used. It has been found that when measurements are being made at high temperatures, care must be taken not to thermally shock the fused quartz buffer because of the possibility of creating permanent strains in the material. If this happens, acoustic impedance discontinuities in the buffer will distort the return echoes. This is especially obvious when the shear mode is being used. Annealing at 1100°C will usually restore the usefulness of the buffer. Crystal quartz buffer rods cut to match the cut of the quartz transducer are useful for low-temperature measurements.

G. Couplant Materials

It is always necessary to use some substance to act as a coupling film between the active area of the buffer rod and the specimen. Nonaq, which has lately gained favor among experimenters, has been found to be only partially satisfactory because it is somewhat hygroscopic and changes consistency during periods of high ambient humidity. It has also been responsible for corrosion of certain specimens. Salol generally produces seals so thin that they require a large γ correction, and for this reason it has been avoided. Dow Corning Resin 276-V9 is very useful for room-temperature measurements using both the longitudinal and shear modes. None of these materials is useful as a couplant at elevated temperatures. For measurements at elevated temperatures, a mixture of calcium carbonate and sodium silicate has been found to be satisfactory. An aqueous solution of sodium silicate with the calcium carbonate in suspension forms upon drying a solid which shows considerable promise as a high-temperature couplant. Recently, measurements were made on a single crystal of α zirconium, using both the shear mode and the longitudinal mode up to a temperature of 755°C. At this temperature the solid couplant was still performing satisfactorily. It can be dissolved in water without

harming the buffer, nor has it damaged any of the specimens used so far, which include crystals of zirconium and uranium. A couplant of the same general type has also been used on single crystals of sodium chloride and silver chloride, but its action on these crystals was not mentioned.(3)

H. Conclusion

The equipment which has been described has shown itself to be simple and convenient enough to allow precise measurements of wave velocity during a continuous rapid change of temperature. It possesses sufficient power output and receiver sensitivity to overcome effects of possible high ultrasonic attenuation in the specimen.

Bibliography

1. McSkimin, H. J., Use of High Frequency Ultrasound for Determining the Elastic Moduli of Small Specimens, IRE Trans. on Ultrasonic Eng., 25, PGUE-5 (1957).

2. Huntington, Emslie, and Hughes, Ultrasonic Delay Lines, J. Franklin Inst. 245, 1, (1948).

3. Stepanov and Eidus, Temperature Dependence of the Elastic Constants Of Monocrystals of Sodium Chloride and Silver Chloride, JETP, 2, 377 (May 1956).

4. Fischer, E. S., The Adiabatic Elastic Moduli of Single-Crystal Alpha Uranium at 25°C, ANL-6096.

5. Fischer, E. S., and Renken, C. J., Adiabatic Elastic Moduli of Single Crystal Alpha Zirconium, to be published in the Journal of Nuclear Materials.

6. Johnson, W. C., Transmission Line Theory, McGraw-Hill Book Co., Inc., New York (1950), p. 95.

Appendix

Analysis for phase angle correction:

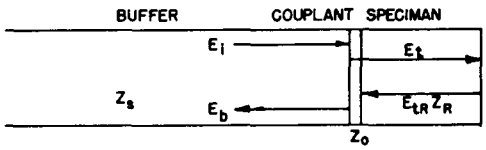

Figure 9

An Idealized Drawing of the Buffer Rod Termination

From transmission line theory,[1] the impedance looking into the couplant from the buffer end is given by

$$Z_d = Z_0 \frac{[(Z_r + Z_0)\, e^{+\gamma l} + (Z_r - Z_0)\, e^{-\gamma l}]}{[(Z_r + Z_0)\, e^{\gamma l} - (Z_r - Z_0)\, e^{-\gamma l}]}$$

$$= Z_0 \frac{(Z_r \cosh \gamma l + Z_0 \sinh \gamma l)}{Z_r \sinh \gamma l + Z_0 \cosh \gamma l} \quad .$$

The reflection from the buffer couplant interface is given by

$$E_b = E_i \frac{Z_d - Z_s}{Z_d + Z_s}$$

where

E_i = incident pressure at the boundary

and

$\frac{Z_d - Z_s}{Z_d + Z_s}$ = reflection coefficient at this boundary for plane waves with the wave front parallel to the boundary.

In the determination of Z_d, the quantity Z_r is considered a pure number, since we are interested at this point in the reflection occurring at the buffer couplant interface before the return of the reflection from the far end of the specimen.

The wave traveling through the seal is given by

$$E_t = \frac{I_s}{2} [(Z_d + Z_0)\, e^{-\gamma x} + (Z_d - Z_0)\, e^{\gamma x}] \quad ,$$

where

$$I_s = \frac{E_s}{Z_d} \qquad E_s = \frac{2Z_d E_i}{Z_s + Z_d}$$

and

$$\frac{2Z_d}{Z_s + Z_d}$$

is the transmission coefficient at this boundary.

The quantity E_t can be put into the form

$$E_t = \frac{2E_i}{Z_s + Z_d} [Z_d \cosh \gamma x - Z_0 \sinh \gamma x] \quad ;$$

at the same specimen couplant interface,

$$E_t = \frac{2E_i}{Z_r + Z_d} [Z_d \cosh \gamma l - Z_0 \sinh \gamma l] \quad .$$

This wave is propagated down the specimen and is reflected from the far end with the reflection coefficient

$$\frac{Z_a - Z_r}{Z_a + Z_r} \approx -1$$

where Z_a is the impedance of air.

Arriving back at the seal, the expression for E_t is given by

$$E_t = \frac{-2E_i}{Z_s + Z_d} [Z_d \cosh \gamma l - Z_0 \sinh \gamma l] e^{-2\gamma_s l_s} \quad ,$$

where γ_s is the propagation constant of the specimen and l_s is the length of specimen.

The impedance looking into the couplant is

$$Z'_d = Z_0 \frac{Z_s \cosh \gamma l + Z_0 \sinh \gamma l}{Z_0 \cosh \gamma l + Z_s \sinh \gamma l} \quad ,$$

and the transmission coefficient at this boundary is $2Z'_d/(Z_s + Z'_d)$.

For the wave propagated back through the seal,

$$E_{tr} = \frac{I_t}{2}\left[(Z'_d + Z_0)\, e^{\gamma d} + (Z'_d - Z_0)\, e^{-\gamma d}\right] e^{-2\gamma_{s^1 s}}$$

$$I_t = \frac{E_{tr}}{Z'_d} \text{ and } E_{tr} = \frac{2Z'_d\, E_t}{Z_r + Z'_d}$$

$$E_{tr} = \frac{-4E_i\,[Z'_d \cosh \gamma d - Z_0 \sinh \gamma d][Z_d \cosh \gamma 1 - Z_0 \sinh \gamma 1]\, e^{-2\gamma_{s^1 s}}}{(Z_r + Z'_d)(Z_s + Z_d)}$$

at d = 1, which is the buffer couplant boundary,

$$E_t = \frac{-4E_i\,[Z'_d \cosh \gamma 1 - Z_0 \sinh \gamma 1][Z_d \cosh \gamma 1 - Z_0 \sinh \gamma 1]\, e^{-2\gamma_{s^1 s}}}{(Z_r + Z'_d)(Z_s + Z_d)}$$

since

$$\frac{E_b}{E_i} = \frac{Z_d - Z_s}{Z_d + Z_s}$$

$$\frac{E_{tr}}{E_b} = \frac{-4[Z'_d \cosh \gamma 1 - Z_0 \sinh \gamma 1][Z_d \cosh \gamma 1 - Z_0 \sinh \gamma 1]\, e^{-2\gamma_{s^1 s}}}{(Z_r + Z'_d)(Z_d - Z_s)}$$

$$\frac{E_{tr}}{E_b} = -4\,\frac{\left[Z_0\,\dfrac{Z_0 \cosh \gamma 1 + Z_0 \sinh \gamma 1}{Z_0 \cosh \gamma 1 + Z_s \sinh \gamma 1} \cosh \gamma 1 - Z_0 \sinh \gamma 1\right]\left[Z_0\,\dfrac{Z_r \cosh \gamma 1 + Z_0 \sinh \gamma 1}{Z_r \sinh \gamma 1 + Z_0 \cosh \gamma 1} \cosh \gamma 1 - Z_0 \sinh \gamma 1\right] e^{-2\gamma_{s^1 s}}}{\left[Z_r + Z_0\,\dfrac{Z_s \cosh \gamma 1 + Z_0 \sinh \gamma 1}{Z_0 \cosh \gamma 1 + Z_0 \sinh \gamma 1}\right]\left[Z_0\,\dfrac{Z_r \cosh \gamma 1 + Z_0 \sinh \gamma 1}{Z_r \sinh \gamma 1 + Z_0 \cosh \gamma 1} - Z_s\right]}$$

After a considerable amount of manipulation and using the identities

$$\cosh^2 x - \sinh^2 x = 1$$

$$2 \sinh x \cosh x = \sinh 2x \quad ,$$

there is obtained

$$\frac{E_{tr}}{E_b} = \frac{-4\, e^{-2\gamma_{s^1 s}}}{\left(\dfrac{Z_r}{Z_s} - \dfrac{Z_s}{Z_r}\right) + \left(\dfrac{Z_0^2}{Z_s Z_r} - \dfrac{Z_s Z_r}{Z_0^2} + \dfrac{Z_r}{Z_s} - \dfrac{Z_s}{Z_r}\right) \sinh^2 \gamma 1 + \sinh 2\gamma 1 \left(\dfrac{Z_0}{Z_s} - \dfrac{Z_s}{Z_0}\right)}$$

If the couplant is considered to be lossless, then $\gamma 1 = j\beta 1$ and

$$\frac{E_{tr}}{E_b} = \frac{-4\, e^{-2\gamma_{s^1 s}}}{\left(\dfrac{Z_r}{Z_s} - \dfrac{Z_s}{Z_r}\right) - \left(\dfrac{Z_0^2}{Z_s Z_r} - \dfrac{Z_s Z_r}{Z_0^2} + \dfrac{Z_r}{Z_s} - \dfrac{Z_s}{Z_r}\right) \sin^2 \beta 1 + j \sin 2\beta 1 \left(\dfrac{Z_0}{Z_s} - \dfrac{Z_s}{Z_0}\right)}$$